Applied Catalysis B: Environmental 145 (2014) 56–62

Contents lists available at ScienceDirect

Applied Catalysis B: Environmental

journal homepage: www.elsevier.com/locate/apcatb

Oxidative steam reforming of bio-butanol for hydrogen production: effects of noble metals on bimetallic CoM/ZnO catalysts (M = Ru, Rh, Ir, Pd)

Weijie Cai[a,b], Pilar Ramírez de la Piscina[a], Narcis Homs[a,b,*]

[a] Departament de Química Inorgànica and Institut de Nanociència i Nanotecnologia, Universitat de Barcelona, Martí i Franquès 1-11, 08028 Barcelona, Spain
[b] Catalonia Institute for Energy Research (IREC), Jardins de les Dones de Negre 1, 08930 Barcelona, Spain

ARTICLE INFO

Article history:
Received 15 October 2012
Received in revised form 11 February 2013
Accepted 5 March 2013
Available online 18 March 2013

Keywords:
Oxidative steam reforming
CoM/ZnO
Hydrogen production
Bio-butanol raw mixture
Bimetallic catalysts

ABSTRACT

The influence of the addition of a noble metal (Ru, Rh, Ir or Pd) on the catalytic performance of Co/ZnO was studied with respect to oxidative steam reforming of the bio-butanol raw mixture (butanol/acetone/ethanol = 6/3/1, mass ratio). Bimetallic catalysts, CoM/ZnO (M = Ru, Rh, Ir, Pd) had higher conversion values, decreased deactivation and higher H_2 concentration in the outlet gas than monometallic Co/ZnO. However, significant differences were found in both raw mixture conversion and H_2 concentrations for the different CoM/ZnO, depending on M. CoRh/ZnO presented the best catalytic behavior (65.1 mol% hydrogen in the outlet after 100 h of reaction at 500 °C with 84% conversion). Characterization of catalysts post-reaction by Raman spectroscopy and TPO showed that less ordered and less abundant carbonaceous deposits were formed over bimetallic catalysts than over the monometallic one; CoRh/ZnO had the lowest amount of such coke.

1. Introduction

It has been proposed that H_2 be used as a new energy carrier in a future. The production of electrical energy using H_2 to feed fuel cells has been contemplated due to issues of efficiency and emissions [1–4]. However, nowadays hydrogen is principally produced by the reformation of fossil fuels, mainly natural gas, and this produces considerable environmental concerns [5,6]. The opportunity to use hydrogen as an environmentally-friendly energy carrier is conditional on the implementation of new methods of H_2 production that use renewable substrates; in the mid-term, the use of biomass-derived substrates could contribute to this goal. Therefore, H_2 production from bio-ethanol, glycerol or dimethyl ether via reformation processes has been widely reported [7–12]. Bio-butanol is emerging as a bioalcohol which is an attractive candidate to be used in the biofuel mix and its availability makes it a potential renewable source for H_2 production. Bio-butanol can be produced via a specific fermentation route which primarily yields a diluted aqueous solution containing approximately 40 wt.% of the raw mixture: butanol/acetone/ethanol = 6/3/1 (mass ratio) [13,14]. To completely remove the water and to obtain separately pure acetone, butanol, and ethanol, an expensive separation process is needed. However, the reformation of the preliminary distillation product to produce hydrogen can be favorable in terms of energy, as no further distillation is necessary. Moreover, the addition of oxygen to the reformation process results in a more favorable energetic balance with respect to the steam reforming process, because the exothermic partial oxidation of the substrates supplies heat for the endothermic steam reforming reaction [15–18]. Oxidative steam reforming (OSR) of the bio-butanol raw mixture could be considered a reasonable compromise between energy balance and hydrogen productivity. Moreover, the presence of oxygen in the OSR process could help with the continuous removal of carbonaceous deposits, and thereby contribute to the stability of the catalysts used.

Thermodynamic analysis of butanol partial oxidation and butanol steam reforming has been reported [19–21] but there are only a few studies of the practical uses of butanol or bio-butanol for H_2 production [22–25]. Our group recently studied steam reforming and OSR of the bio-butanol raw mixture over cobalt-based catalysts [22–24]. We demonstrated that the addition of a small amount of iridium (0.3 wt.%) improved the catalytic performance of a Co/ZnO catalyst (7 wt.% Co) in OSR of the raw mixture. Both the H_2 yield and the resistance to coke formation were higher for CoIr/ZnO than for Co/ZnO or Ir/ZnO (1 wt.% Ir) monometallic catalysts. However, a CoIr/ZnO catalyst containing a higher amount of Ir (0.9 wt%)

* Corresponding author at: Universitat de Barcelona; Departament de Química Inorgànica and Institut de Nanociència i Nanotecnologia; Martí i Franquès 1-11; 08028 Barcelona; Spain. Tel.: +34 934037056; fax: +34 934907725.
E-mail addresses: narcis.homs@qi.ub.es, nhoms@irec.cat (N. Homs).

0926-3373/$ – see front matter © 2013 Elsevier B.V. All rights reserved.
http://dx.doi.org/10.1016/j.apcatb.2013.03.016

showed poorer catalytic behavior in the OSR of the raw mixture; in the last catalyst, we found separated Ir^0 clusters that were interacting with the support [23]. Taking into account this background, in the research reported here, we carried out an in-depth study of the effect of the addition of small amounts of different noble metals (0.2–0.3 wt.% M) to form CoM/ZnO catalysts (M = Ru, Rh, Ir, Pd) with respect to the OSR of the bio-butanol raw mixture. The aim of the work is to devise a novel catalyst that efficiently produces hydrogen from bio-butanol raw mixture. Therefore, special attention was paid to the deactivation of the catalysts and to the generation of carbon deposits. In order to compare the catalysts properly, they were tested under conditions in which the initial conversion was lower than 100% for all them and the carbonaceous deposits were characterized by Raman spectroscopy and temperature-programmed oxidation (TPO).

2. Experimental

2.1. Catalyst preparation

CoM/ZnO (M = Ru, Rh, Pd) were prepared by one-step incipient wetness co-impregnation using a similar method to that reported previously for the preparation of CoIr/ZnO and Co/ZnO [23]. The ZnO support (41 m^2/g) was purchased from TECNAN. The metallic precursors used were $Co(NO_3)_2{\cdot}6H_2O$, $RuCl_3$, $RhCl_3$ and $PdCl_2$. CoM/ZnO catalysts, containing around 7 wt.% Co and 0.2–0.3 wt.% noble metal, were prepared. The impregnated samples were dried at 70 °C overnight and then calcined at 450 °C for 5 h.

2.2. Catalyst characterization

The metal contents were analyzed using inductively-coupled plasma atomic emission spectrometry analysis (ICP-OES Perkin Elmer Optima 3200RL).

N_2 adsorption-desorption isotherms were obtained at −196 °C using Tristar-II Micromeritics apparatus. Prior to measurement, the samples were outgassed at 150 °C for 2 h. The specific surface area was calculated by multipoint BET analysis of the nitrogen adsorption isotherms.

X-ray diffraction (XRD) patterns were recorded using a Siemens D-500 X-ray diffractometer with nickel-filtered CuKα_1 radiation. XRD profiles were collected between 2θ = 20–100°, using a step width of 0.05° and counting 3 s at each step. The mean crystallite sizes of the cobalt species were calculated according to the Debye–Scherrer equation.

Hydrogen temperature-programmed reduction (TPR) was performed with a Micromeritics AutoChem II chemisorption analyzer. 20 mg of the sample was pretreated at 90 °C for 30 min under flowing He (50 mL/min). After cooling to room temperature, the samples were fed with a flow of 12 vol% H_2/Ar (50 mL/min) and temperature was linearly increased at a rate of 10 °C/min up to 800 °C.

The in situ diffuse reflectance infrared spectroscopy (DRIFT) results of carbon monoxide adsorption were recorded using a Nicolet Magna-IR 750 FTIR spectrometer equipped with a liquid-nitrogen-cooled MCT detector and a Spectra Tech catalytic chamber. The recorded spectra consisted of 64 scans at 4 cm^{-1} resolution. Prior to CO adsorption, the samples were reduced ex situ at 450 °C under a 10 vol% H_2/Ar mixture for 1.5 h and then they were re-reduced in the catalytic chamber under a flow of 16 mL/min (12 vol% H_2/Ar) at 400 °C and cooled to room temperature under a He flow (18 mL/min). Carbon monoxide (10 vol% CO/He, 18 mL/min) was brought into contact with the reduced catalysts at room temperature and then the samples were outgassed with He (18 mL/min) at room temperature. The spectra were referred to the corresponding background spectrum of the reduced catalyst.

The TPO experiments were performed on used catalysts using a Micromeritics AutoChem II chemisorption analyzer equipped with a continuous-flow fixed-bed quartz reactor. About 40 mg of the used catalysts was heated (10 °C/min) from room temperature to 820 °C under an O_2/He flow (10 vol%, 50 mL/min). Oxygen consumption was measured using a thermal conductivity detector (TCD). The deposited carbon was determined after the catalytic test from total O_2 consumption, by subtraction of the amount of O_2 necessary for the re-oxidation of the metallic phases. Then, the amount of coke formed was referred to the amount of catalyst and the time on-stream.

Raman spectra were collected with a Jobin-Yvon T64000 spectrometer equipped with a CCD detector. The samples were excited with the 532.1 nm Ar line and spectrum acquisition consisted of three accumulations of 180 s for each sample. The laser power was limited to 0.7 mV to minimize laser-heating effects.

2.3. Catalytic measurements

Catalytic reforming tests were carried out at atmospheric pressure in a Microactivity-Reference unit (PID Eng&TECH). The catalyst was mixed with inactive SiC (Prolabo, 0.5 mm) and placed in a tubular fixed-bed reactor (305 mm long, 9 mm i.d., 316-L stainless steel) up to a catalytic volume of approximately 1 mL. The gas hourly space velocity (GHSV) used was 7500 h^{-1} and the reaction temperature was 500 °C. The temperature was measured using a thermocouple in direct contact with the catalytic bed. Prior to the catalytic reaction, the catalysts were reduced in situ under a 10 vol% H_2/Ar mixture at 450 °C for 1.5 h. Two piston pumps were used to introduce the liquid raw mixture (butanol/acetone/ethanol = 6/3/1, mass ratio) and water separately, and these were then vaporized and mixed with a controlled flow of dilution gas (Ar) and air. The molar composition of the reactant feed was: raw mixture/water/air/Ar = 1/10/7.5/12. The products were analyzed on-line with a Varian 450-GC equipped with a methanizer and TCD and FID detectors. The carbon balance between the outlet gas and the reactant inlet was ≤3%.

3. Results and discussion

As stated above, the OSR of bio-butanol raw mixture over CoM/ZnO catalysts (M = Ir, Rh, Ru, Pd) containing small amounts of M (0.2–0.3 wt.% M) was studied and the results were compared with those obtained over the monometallic Co/ZnO catalyst. Table 1 shows several characteristics of the catalysts. It can be seen from Table 1 that after calcination, the catalysts had similar surface areas (15–18 $m^2\ g^{-1}$). The XRD patterns of calcined catalysts (not shown) only exhibited diffraction peaks corresponding to the ZnO support (JCPDS 03-065-3411) and Co_3O_4 (JCPDS 01-080-1544); with no significant differences between the XRD patterns of the bimetallic and monometallic catalysts. This is probably due to the light noble metal loading. The crystallite sizes of Co_3O_4 and ZnO determined from the Debye–Scherrer equation were in the ranges 9–11 nm and 28–34 nm respectively (see Table 1).

Fig. 1 compares the TPR profiles of catalysts. Although we have recently reported TPR profiles of Co/ZnO and CoIr/ZnO [23], they are included in Fig. 1 for comparison with profiles of the other bimetallic catalysts. The TPR profiles of CoM/ZnO showed two separate reduction peaks, which may be related to those in the TPR profile of Co/ZnO; the peaks in the latter correspond to the reduction of Co_3O_4 to CoO and of CoO to Co^0. As expected, the TPR profiles of all the CoM/ZnO showed reduction peaks at lower temperatures than Co/ZnO did, with CoRh/ZnO being the sample that showed

Table 1
Several characteristics of CoM/ZnO and Co/ZnO catalysts.

Catalyst	S_{BET}[a] (m^2/g)	Composition (wt.%)		Co_3O_4 d[b] (nm) (calcined)	Co d[b] (nm) (used)	ZnO d[b] (nm) (calcined)	ZnO d[b] (nm) (used)
		Co	M				
Co/ZnO	15	7.17	–	10	28	34	45
CoIr/ZnO	17	7.20	0.30	11	19	31	41
CoRh/ZnO	17	6.70	0.19	9	14	28	40
CoRu/ZnO	18	6.71	0.20	10	19	30	41
CoPd/ZnO	17	6.63	0.26	11	21	32	43

[a] BET surface-area of calcined catalysts.
[b] Crystallite sizes were calculated from XRD patterns of calcined and post-reaction catalysts using the Debye–Scherrer equation.

reduction peaks at the lowest temperatures. Moreover, it was not possible to distinguish separate well-defined peaks which could be assigned to the corresponding MO_x reduction. MO_x should initially be reduced and then M should facilitate the reduction of the cobalt species due to hydrogen spillover [26,27].

The amount of H_2 consumed during the TPR experiments of CoM/ZnO largely exceeded (approximately 21–26%) the theoretical consumption of H_2 necessary for reducing Co_3O_4 and MO_x (M = Ru, Rh and Pd), this is related to the partial reduction of the support. Similar behavior was recently reported for CoIr/ZnO [23]. For Co/ZnO the H_2 consumed corresponded to that expected for the Co_3O_4 reduction.

In order to characterize the nature of surface metallic sites of fresh catalysts, CO chemisorption on reduced catalysts was followed by in situ DRIFT. Carbon monoxide is an appropriate probe molecule which has been used to study the nature of metallic surface sites in both mono-metallic and bi-metallic cobalt-based catalysts [10,23,26,28,29]. Fig. 2 shows the spectra registered after CO adsorption on CoRu/ZnO, CoRh/ZnO and CoPd/ZnO catalysts. The spectrum obtained for CoRu/ZnO shows a very broad main band with two maxima centered at 2037 and 1980 cm^{-1}. The band is related to the overlapping of bands due to CO linearly bonded to Co^0 and Ru^0 [23,26,29]. Below 1900 cm^{-1}, only very low intensity bands could be detected; that indicates that the presence of the surface noble metal strongly diminished the number of bridged CO molecules on the Co. Moreover, there are no bands above 2100 cm^{-1} and this indicates the absence of oxidized Co-surface species on CoRu/ZnO in accordance with the easy reducibility of CoRu/ZnO. These results are in line with those reported for the CoIr/ZnO catalyst [23]. After CO adsorption on the CoRh/ZnO catalyst, well-defined bands could be observed with maxima at 2107 and 2024 cm^{-1}. The presence of these two bands indicates the presence of surface geminal dicarbonyl species $[Rh(CO)_2]^+$. The adsorption of CO on small Rh entities results in the formation of these species, which are characterized by υ_s(CO) at 2120–2075 cm^{-1} and υ_{as}(CO) at 2053–1990 cm^{-1}; the presence of this type of species has already been proposed for CoRh based catalysts supported on CeO_2-ZrO_2 [10]. A shoulder at approximately 2059 cm^{-1} and weaker absorptions at approximately 1943 cm^{-1} and 1838 cm^{-1} can be also observed. Linearly bonded CO on metallic centers, Rh and/or Co could yield bands around 2059 cm^{-1}. However, the simultaneous presence of bands at 1943 cm^{-1} and 1838 cm^{-1} together with the band at approximately 2059 cm^{-1} could indicate the presence of $[Co(CO)_4]^-$ species coming from the disproportionation of cobalt carbonyl species resulting from the adsorption of CO on very small cobalt entities [30]. For this catalyst, no bands which could be assigned to the presence of oxidized surface cobalt species were found. Finally, a more complex infrared spectrum was obtained for CoPd/ZnO. The spectrum is dominated by a band centered at 1941 cm^{-1}. Taking into account the considerable tendency of Pd to coordinate CO in a bridging way and the relative intensity of the 1941 cm^{-1} absorption, this band could be assigned to a bridged coordination of CO on Pd^0 [31]. This could indicate that Pd^0 agglomerates exist on the surface of CoPd/ZnO. The broad band centered at 2055 cm^{-1} corresponds to the presence of CO linearly coordinated to metallic centers. Moreover, a band at a higher wavenumber (2178 cm^{-1}) can also be observed. This band is related to the presence of surface oxidized ($Co^{\delta+}$) species. So for CoPd/ZnO, the presence of separate Co and Pd aggregates could be proposed from CO adsorption experiments.

The behavior of catalysts in the OSR of bio-butanol raw mixture was determined over 100 h. The reaction conditions used were chosen in order to facilitate a proper comparison of the deactivation of

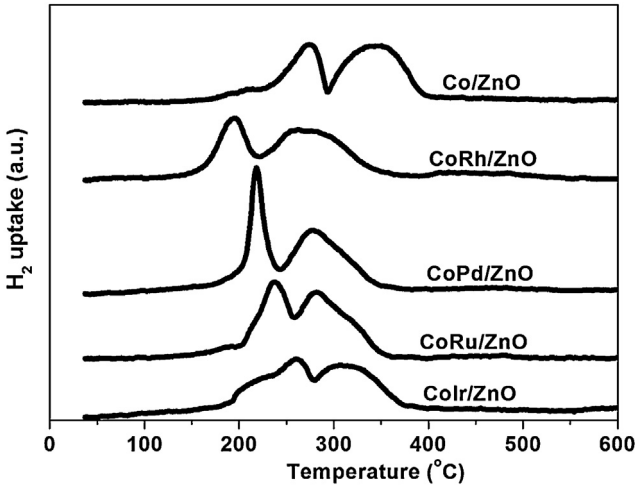

Fig. 1. TPR profiles of calcined CoM/ZnO and Co/ZnO catalysts.

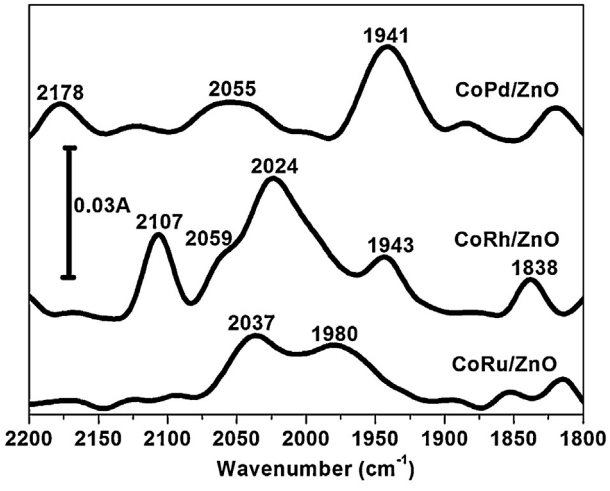

Fig. 2. In situ DRIFT spectra of reduced catalysts after CO chemisorption and He-flushing at room temperature.

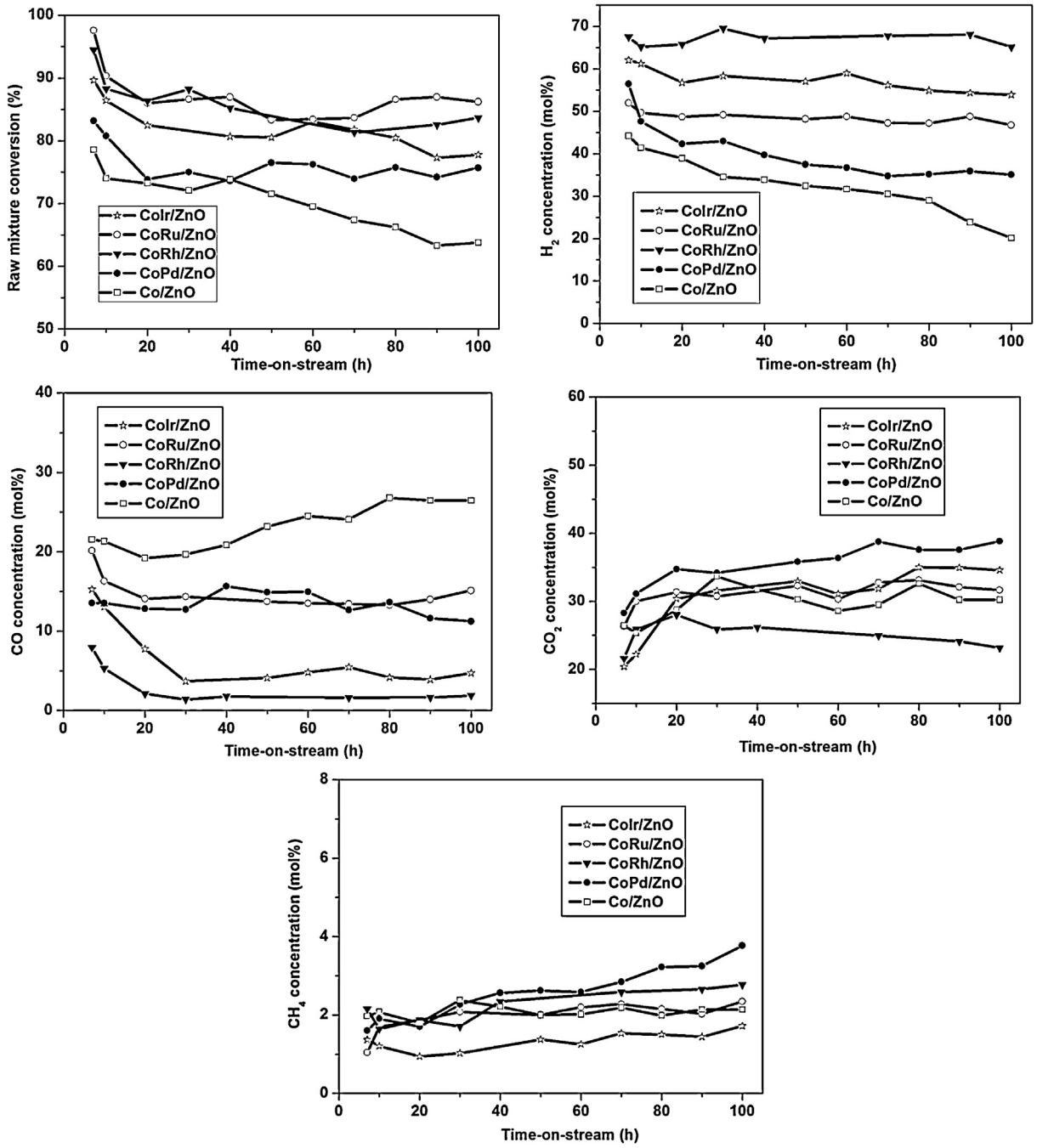

Fig. 3. Catalytic behavior in the OSR of the raw mixture over CoM/ZnO and Co/ZnO catalysts. Molar concentration of H_2, CO_2, CO and CH_4 in the dry outlet gas is shown considering all products obtained and unconverted reactants. Reaction conditions: $T = 500\,^{\circ}C$; S/C = 3; butanol/acetone/ethanol = 6/3/1, mass ratio; raw mixture/O_2 = 1/1.5, molar ratio; 300 mg catalyst; GHSV = 7500 h^{-1}.

the catalysts. For this reason, in all cases the initial raw mixture conversion was lower than 100%. The development of stable catalysts is one of the most important issues in the production of hydrogen from bio-alcohols [1].

Fig. 3 presents the behavior of catalysts in the OSR of the bio-butanol raw mixture at 500 °C. Values for initial conversion ($t = 7$ h) of the raw mixture were in the range 79%-98%; the lowest and the highest value of initial conversion corresponded to Co/ZnO and CoRu/ZnO, respectively. After 100 h on-stream, bimetallic catalysts showed 9–13% deactivation, with the greatest deactivation occurring during the first 20 h. In contrast, Co/ZnO showed continuous deactivation throughout the 100 h of the study, with a total deactivation of 20%. In all cases, the major component of the raw mixture in the outlet gas was acetone. This study did not allow us to establish whether, the acetone found in the outlet gas was formed from ethanol through dehydrogenation and aldol condensation reactions, or it was unconverted acetone [2].

The main reaction products were H_2, CO_2, CO, CH_4, C_2H_4 and butyraldehyde. The distribution of H_2, CO_2, CO and CH_4 in the dry outlet gas (expressed in % molar concentration considering all the products formed and unconverted reactants) is shown in Fig. 3 as a function of time on-stream. The initial and final molar concentration of ethylene and butyraldehyde are shown in Fig. 4. With respect to the H_2 production, all the bimetallic catalysts showed higher values than Co/ZnO (Fig. 3). Over Co/ZnO, the H_2 concentration, which progressively decreased over time, ranged from 44.1 mol%

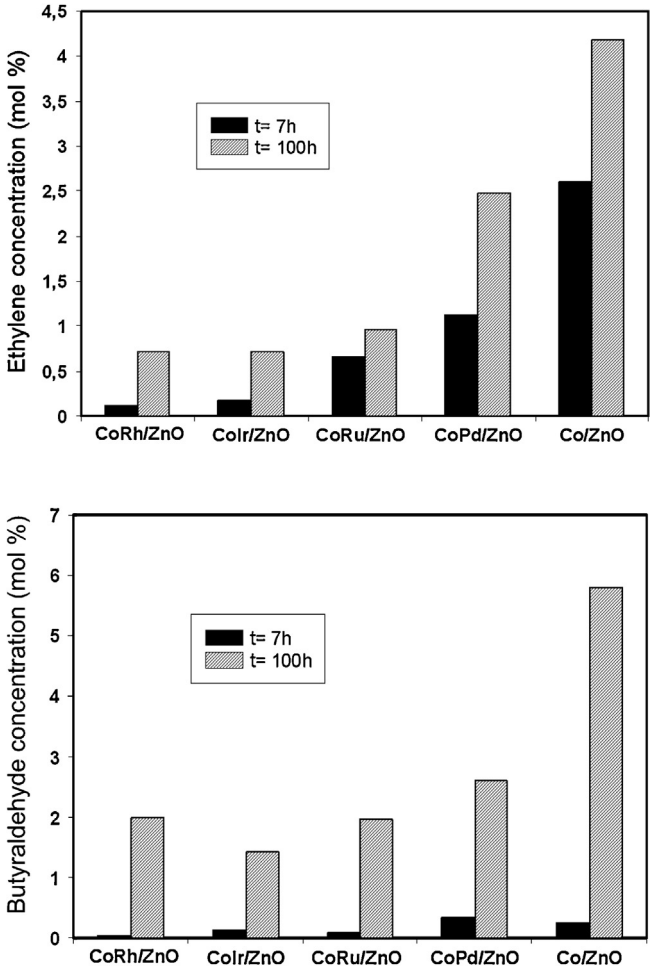

Fig. 4. Ethylene and butyraldehyde molar concentration (%) in the outlet dry gas obtained in the OSR of the raw mixture over CoM/ZnO and Co/ZnO catalysts at initial (t = 7 h) and final (t = 100 h) reaction time. Reaction conditions: T = 500 °C; S/C = 3; butanol/acetone/ethanol = 6/3/1, mass ratio; raw mixture/O_2 = 1/1.5, molar ratio; 300 mg catalyst; GHSV = 7500 h^{-1}.

(t = 7 h) to 20.1 mol% (t = 100 h). In contrast, the profiles of H_2 concentration obtained over CoRh/ZnO, CoIr/ZnO and CoRu/ZnO were almost constant, particularly after 20 h on-stream. However, the H_2 concentration obtained over CoPd/ZnO showed a progressive decline over time; after 100 h of reaction, a hydrogen concentration of approximately 35 mol% was obtained over CoPd/ZnO. The highest H_2 concentration was obtained over CoRh/ZnO: 65.1 mol% after 100 h of reaction. CoRh/ZnO also showed the lowest CO concentration in the effluent; after the first 20 h on-stream and up until the end of the catalytic test (100 h), the value remained below 2 mol%.

Fig. 3 also shows the evolution of CH_4, which increased for all the catalysts over time; this is probably related to a slight decline in the methane steam reforming capacity of the catalysts. CoPd/ZnO was the catalyst which showed both the highest increase in CH_4 concentration over time and the highest CH_4 concentration after 100 h on-stream (3.8 mol%). As stated above, all catalysts produced small amounts of ethylene; the ethylene concentration obtained over bimetallic catalysts was lower than that obtained over Co/ZnO (see Fig. 4). After 100 h under reaction conditions, CoRh/ZnO and CoIr/ZnO showed the lowest ethylene concentration in the effluent. This is significant because ethylene has been identified as a precursor of stable polymeric coke that can be deposited on the active phase leading to catalyst deactivation [32,33]. Fig. 4 also shows that the butyraldehyde concentration obtained over bimetallic catalysts were lower than that obtained over Co/ZnO; aldehydes have been

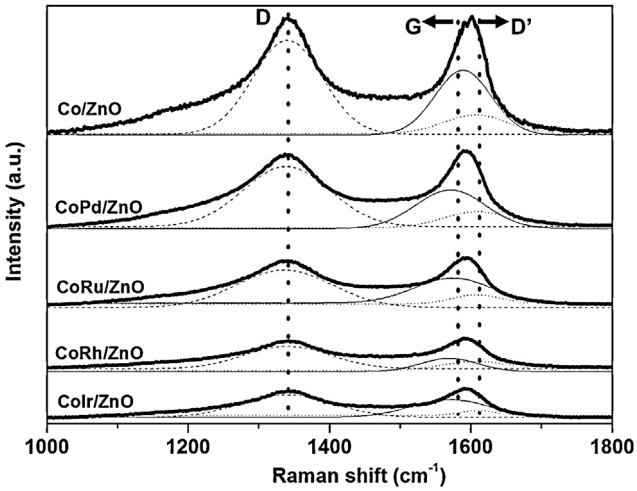

Fig. 5. Raman spectra of CoM/ZnO and Co/ZnO post-reaction catalysts.

proposed as intermediates in reforming processes and as precursors of coke formation [33].

Post-reaction catalysts were characterized by XRD, TPO and Raman spectroscopy. In the XRD patterns of CoM/ZnO post-reaction catalysts (not shown), in addition to the diffraction peaks of the ZnO support (JCPDS 03-065-3411), only a low intensity peak at 2θ = 44.2° was observed which corresponds to Co_{fcc}(1 1 1): the most intense reflection of the Co_{fcc} phase (JCPDS 00-015-0806). In the XRD pattern of Co/ZnO used-catalyst (not shown), in addition to the above mentioned peaks, a peak at 2θ = 42.2° assigned to the presence of CoO phase (JCPDS 00-009-0402) was found. Although for all the catalysts the Co_{fcc} particle size calculated from the Debye–Scherrer equation (Table 1) was higher than the size determined for Co_3O_4 in the corresponding calcined catalyst, the CoM/ZnO catalysts showed smaller Co_{fcc} particles than Co/ZnO. The crystallite size of ZnO after catalytic tests (40–45 nm) was also in all cases higher than that determined for calcined catalysts but there was no significant difference between the ZnO sizes in different catalysts (Table 1).

The addition of a noble metal favors the stabilization of the Co^0 phase during OSR and reduces the crystallization of cobalt species during the reduction and/or reaction, and this could contribute to better behavior of the catalysts and to their higher initial activity and/or stability [26,27].

Bearing in mind that coke formation is considered a main cause of catalyst deactivation in alcohol reformation processes, the nature and characteristics of carbon deposits on the post-reaction catalysts were studied by Raman spectroscopy and TPO experiments. Fig. 5 shows the Raman spectra of catalysts after the stability test (100 h) in the 1000–1800 cm^{-1} zone. Two distinct bands with maxima at approximately 1340 cm^{-1} and 1600 cm^{-1} appeared for all the samples. The former (D band) is ascribed to poorly structured carbon deposits. However, two components are usually distinguished in the band at approximately 1600 cm^{-1}: the component at 1575–1600 cm^{-1} is due to the in-plane sp^2 carbon–carbon stretching vibrations of well structured coke or graphite-like structures; and the component at 1600–1620 cm^{-1} (D' component) indicates the occurrence of less ordered deposits [34–36]. For a proper discussion of the results, Fig. 5 shows the deconvolution of the band at approximately 1600 cm^{-1} into its G and D' components; this allowed us to determine I_G and calculate the I_G/I_D values. The ratio between the areas of the G and D bands, I_G/I_D, is considered to be an index of the degree of graphitization of carbonaceous deposits [34–36]; that is, the higher I_G/I_D, the greater the degree of graphitization of the carbon. The values of I_G/I_D obtained are shown

Table 2
Index of graphitization of carbonaceous deposits on post reaction catalysts. I_G/I_D ratio and position of G band (P_G) obtained from Raman spectra analysis.

Catalyst	I_G/I_D	P_G (cm^{-1})
Co/ZnO	0.54	1583
CoIr/ZnO	0.31	1575
CoRh/ZnO	0.24	1576
CoRu/ZnO	0.41	1578
CoPd/ZnO	0.45	1576

in Table 2; Co/ZnO showed the highest I_G/I_D, indicating the formation of more ordered carbon deposits over Co/ZnO than over the bimetallic samples. CoIr/ZnO and CoRh/ZnO had the lowest I_G/I_D values: 0.31 and 0.24 respectively. Moreover, the position of the G band (P_G) has also been related to the degree of graphitization of carbonaceous deposits; a higher P_G indicates a higher degree of graphitization [34,36]. The P_G values of bimetallic catalysts (Table 2) were in all cases lower than that of Co/ZnO, this can be related to a lower degree of graphitization of carbon deposits obtained over bimetallic samples according with the I_G/I_D values obtained.

Fig. 6 shows the TPO profiles of the post-reaction catalysts. The profiles of oxygen consumption of the CoM/ZnO bimetallic catalysts clearly differ from that of Co/ZnO. CoM/ZnO post-reaction catalysts showed profiles with a maximum of oxygen consumption below 450 °C and a tail that extended out at higher temperatures; this was the major component for CoPd/ZnO. In contrast, Co/ZnO showed a well-defined peak, with a maximum at 475 °C and a small peak at approximately 570 °C. Taking into account that a higher temperature for the removal of carbonaceous deposits is related to a higher order, the TPO results are in accordance with the Raman analysis which indicated the presence of more ordered carbonaceous deposits on Co/ZnO than on CoM/ZnO. Fig. 6 also shows a quantification of the oxygen consumed during the TPO experiments due to the oxidation of the carbon deposits generated on the catalysts. CoM/ZnO catalysts exhibited less coke than Co/ZnO and the lowest amount of carbonaceous residues was formed on CoRh/ZnO; a similar trend was observed for the ethylene and butyraldehyde concentration in the outlet gas during the catalytic test (Fig. 4).

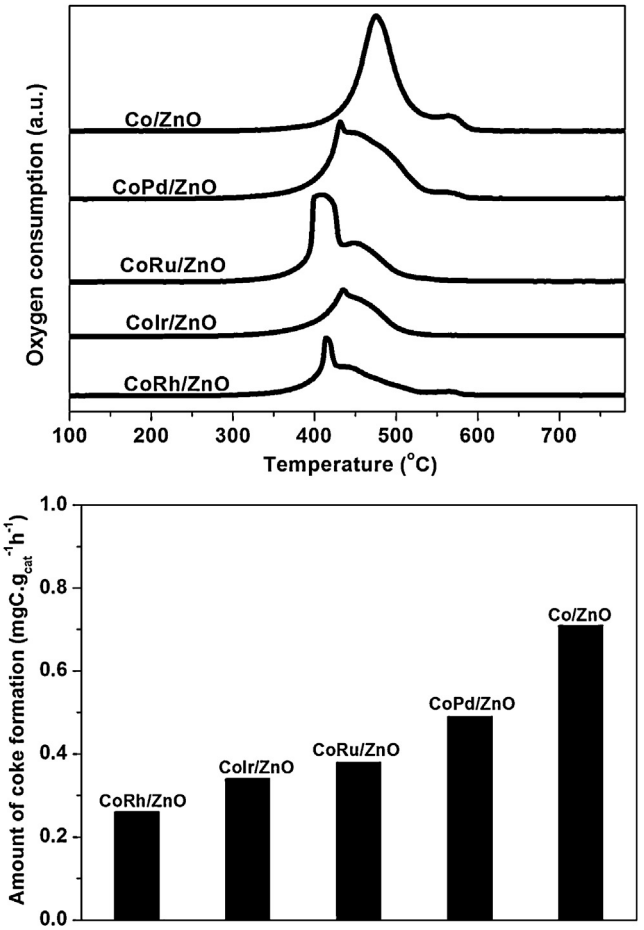

Fig. 6. TPO profiles of post-reaction catalysts and quantification of the corresponding amount of coke.

These characterization results indicated that the addition of a noble metal decreased catalyst deactivation by stabilizing Co^0 phase, preventing active metal sintering and simultaneously inhibiting detrimental coke formation, compared to the monometallic catalyst. The stabilization of Co^0 phase has been pointed of great relevance for improvement on catalytic behavior of Co-based catalysts for ethanol reforming [37].

4. Conclusions

A series of CoM/ZnO catalysts doped with M (M = Ru, Rh, Ir or Pd) were tested in the OSR of the bio-butanol raw mixture containing acetone, ethanol and butanol to produce hydrogen. The addition of the noble metal (M) greatly improved the catalytic performance of the monometallic Co/ZnO catalyst. The effect of M is related to the increase of reducibility of catalyst and the decrease of both cobalt sintering and carbon deposits under OSR conditions. The effect is higher for ZnO-supported CoM catalysts with M belonging to group 9 (Rh, Ir). CoRh/ZnO exhibited the best catalytic behavior compared to the other samples studied, showing the highest production of hydrogen and the lowest amount of carbon deposits. On CoRh/ZnO, the presence of small Co and Rh entities was determined. The OSR of the bio-butanol raw mixture over the CoRh/ZnO catalyst yielded 65.1 mol% hydrogen concentration in the outlet gas after 100 h on-stream at 500 °C at 84% raw mixture conversion.

Acknowledgements

The authors are grateful to Consolider Ingenio 2010, Multicat CSD2009-00050, MAT2011-23775, ACENET-ACE.07.009 (CTQ2008-02961-E) and 2009SGR-0674 projects for financial support.

References

[1] L.V. Mattos, G. Jacobs, B.H. Davis, F.B. Noronha, Chemical Reviews 112 (2012) 4094–4123.
[2] P. Ramírez de la Piscina, N. Homs, Chemical Society Reviews 37 (2008) 2459–2467.
[3] R.M. Navarro, M.A. Peña, J.L.G. Fierro, Chemical Reviews 107 (2007) 3952–3991.
[4] D.K. Liguras, D.I. Kondarides, X.E. Verykios, Applied Catalysis B 43 (2003) 345–354.
[5] H.F. Abbas, W.M.A. Wan Daud, International Journal of Hydrogen Energy 35 (2010) 1160–1190.
[6] A.M. Amin, E. Croiset, W. Epling, International Journal of Hydrogen Energy 36 (2011) 2904–2935.
[7] M. Araque, L.M. Martínez, J.C. Vargas, M.A. Centeno, A.C. Roger, Applied Catalysis B 125 (2012) 556–566.
[8] S.M. de Lima, A.M. da Silva, L.O.O. da Costa, J.M. Assaf, L.V. Mattos, R. Sarkari, A. Venugopal, F.B. Noronha, Applied Catalysis B 121–122 (2012) 1–9.
[9] W. Cai, F. Wang, A. van Veen, C. Descorme, Y. Schuurman, W. Shen, C. Mirodatos, International Journal of Hydrogen Energy 35 (2010) 1152–1159.
[10] E.B. Pereira, P. Ramírez de la Piscina, S. Marti, N. Homs, Energy & Environmental Science 3 (2010) 487–493.
[11] Q. Zhang, F. Du, X. He, Z. Liu, Y. Zhou, Catalysis Today 146 (2009) 50–56.
[12] R.M. Navarro, M.C. Álvarez-Galván, M. Cruz Sánchez-Sánchez, F. Rosa, J.L.G. Fierro, Applied Catalysis B 55 (2005) 229–241.
[13] V. García, J. Päkkilä, H. Ojamo, E. Muurinen, R.L. Keiski, Renewable & Sustainable Energy Reviews 15 (2011) 964–980.
[14] C. Jin, M. Yao, H. Liu, C. Lee, J. Ji, Renewable & Sustainable Energy Reviews 15 (2011) 4080–4106.

[15] W. Cai, F. Wang, E. Zhan, A. van Veen, C. Mirodatos, W. Shen, Journal of Catalysis 257 (2008) 96–107.
[16] W. Cai, F. Wang, C. Danie, A. van Veen, W. Shen, C. Mirodatos, Journal of Catalysis 286 (2012) 137–152.
[17] M.H. Youn, J.G. Seo, H. Lee, Y. Bang, J.S. Chung, I.K. Song, Applied Catalysis B 98 (2010) 57–64.
[18] G.B. Sun, K. Hidajat, X.S. Wu, S. Kawi, Applied Catalysis B 81 (2008) 303–312.
[19] W. Wang, Y. Cao, International Journal of Hydrogen Energy 35 (2010) 13280–13289.
[20] G.A. Nahar, S.S. Madhani, International Journal of Hydrogen Energy 35 (2010) 98–109.
[21] W. Wang, Y. Cao, International Journal of Hydrogen Energy 36 (2010) 2887–2895.
[22] W. Cai, P. Ramírez de la Piscina, N. Homs, Bioresource Technology 107 (2012) 482–486.
[23] W. Cai, N. Homs, P. Ramírez de la Piscina, Green Chemistry 14 (2012) 1035–1043.
[24] W. Cai, P. Ramírez de la Piscina, K. Gabrowska, N. Homs, Bioresource Technology 128 (2013) 467–471.
[25] F. Bimbela, M. Olive, J.R.L. Garcia, J. Arauzo, Journal of Analytical and Applied Pyrolysis 85 (2009) 204–213.
[26] E.B. Pereira, N. Homs, S. Marti, J.L.G. Fierro, P. Ramírez de la Piscina, Journal of Catalysis 257 (2008) 206–214.
[27] L.P.R. Profeti, E.A. Ticianelli, E.M. Assaf, Journal of Power Sources 175 (2008) 482–489.
[28] A.Y. Khodakov, W. Chu, P. Fongarland, Chemical Reviews 107 (2007) 1692–1744.
[29] A.A. Khassin, T.M. Yurieva, V.V. Kaichev, V.I. Bukhtiyarov, A.A. Budneva, E.A. Paukshtis, V.N. Parmon, Journal of Molecular Catalysis A 175 (2001) 189–204.
[30] J. Llorca, P. Ramirez de la Piscina, J.A. Dalmon, J. Sales, N. Homs, Applied Catalysis B 43 (2003) 355–369.
[31] N. Sheppard, T.T. Nguyen, in: R.J. Clark, R.E. Hester (Eds.), Advances in Infrared and Raman Spectroscopy, vol. 5, Wiley, New York, 1978 (Chapter 2).
[32] A.J. Vizcaino, A. Carrero, J.A. Calles, International Journal of Hydrogen Energy 32 (2007) 1450–1461.
[33] F. Romero-Sarria, J.C. Vargas, A.C. Roger, A. Kiennemann, Catalysis Today 133–135 (2008) 149–153.
[34] P. Lespade, A. Marchand, M. Couzy, F. Cruege, Carbon 22 (1984) 375–385.
[35] Y. Li, B. Zhang, X. Xie, J. Liu, Y. Xu, W. Shen, Journal of Catalysis 238 (2006) 412–424.
[36] B. Valle, P. Castaño, M. Olazar, J. Bilbao, A.G. Gayubo, Journal of Catalysis 285 (2012) 304–314.
[37] A.M. Karim, Y. Su, M.H. Engelhard, D.L. King, Y. Wang, ACS Catalysis 1 (2011) 279–286.